Defect engineering of single- and few-layer MoS 2 by swift heavy ion irradiation

Lukas Madauss, Oliver Ochedowski, Henning Lebius, Brigitte Ban-D'etat, Carl Naylor, A Johnson, Jani Kotakoski, Marika Schleberger

Defect engineering of single- and few-layer MoS_2 by swift heavy ion irradiation

2D Materials

OPEN ACCESS

RECEIVED
19 August 2016

REVISED
11 November 2016

ACCEPTED FOR PUBLICATION
25 November 2016

PUBLISHED
12 December 2016

PAPER

Defect engineering of single- and few-layer MoS_2 by swift heavy ion irradiation

Lukas Madauß[1], Oliver Ochedowski[1], Henning Lebius[2], Brigitte Ban-d'Etat[2], Carl H Naylor[3], A T Charlie Johnson[3], Jani Kotakoski[4] and Marika Schleberger[1]

[1] Fakultät für Physik and CENIDE, Universität Duisburg-Essen, D-47057 Duisburg, Germany
[2] CIMAP, (CEA-CNRS-ENSICAEN-UCN), F-14070 Caen, France
[3] Department of Physics and Astronomy, University of Pennsylvania, 19104 PA, USA
[4] Faculty of Physics, University Vienna, A-1090 Vienna, Austria

E-mail: marika.schleberger@uni-due.de

Keywords: MoS_2, defects, irradiation

Abstract

We have investigated the possibility to use swift heavy ion irradiation for nano-structuring supported and freestanding ultra-thin MoS_2 samples. Our comprehensive study of the ion-induced morphological changes in various MoS_2 samples shows that depending on the irradiation parameters a multitude of extended defects can be fabricated. These range from chains of nano-hillocks in bulk-like MoS_2, and foldings in single and bilayer MoS_2, to unique nano-incisions in supported and freestanding single layers of MoS_2. Our data reveals that the primary mechanism responsible for the incisions in the ultrathin supported samples is the indirect heating by the SiO_2 substrate. We thus conclude that an energy of less than 2 keV per nm track length is sufficient to fabricate nano-incisions in MoS_2 which is compatible with the use of the smallest accelerators.

1. Introduction

Two-dimensional (2D) materials are at the center of many novel technologies, including but not limited to energy conversion, opto- and flexible electronics and biomedical applications [1, 2]. The most part of these concepts relies heavily on the possibility to engineer the 2D material in one way or the other. In particular, for potential breakthrough applications such as water desalination and DNA sequencing with the help of synthetic nano-pores [3, 4], or manipulating catalytic [5], optical [6] and thermoelectric [7] properties based on specific sample nanostructures, defect engineering on the nanoscale is the key to success. Therefore several experimental and theoretical studies have looked into the effect of defects on the optical and electronic properties of transition metal dichalcogenides (TMDCs), seen as promising building blocks for future applications. While point-like defects can be introduced into TMDCs rather easily by ion [8] and electron bombardment [9], or plasma treatment [10], the artificial introduction of extended defects is not so easy. One of the most powerful tools for defect engineering of surfaces and bulk materials at the atomic scale is the irradiation with swift heavy ions (SHI) [11]. SHI are projectiles with a typical energy of around 1 MeV per atomic mass unit. Their interaction with matter is governed by electronic excitation rather than nuclear collisions (for a review see e.g. [12]). As a consequence, and in stark contrast to keV ions, a SHI may modify the material inside a very narrow (a few nanometres) and extended volume (up to several microns) centered around its trajectory before it is finally stopped. Therefore, using SHI irradiation under grazing incidence, extremely elongated modifications, so-called surface tracks, may be created at the surface of a given material. These may manifest themselves e.g. in the form of chains of nanosized hillocks in dielectrics such as $SrTiO_3$ [13], or as narrow, one-atom deep trenches as in SiC [14], or as foldings in graphene and MoS_2, respectively [15, 16]. Despite the recent successful applications of SHI irradiation in the exciting and rapidly growing field of nanostructured 2D materials, a systematic understanding of the relevant processes is still lacking. This deficiency hampers quantitative predictions as well as a systematic and efficient exploitation of SHI

irradiation for nanostructuring 2D materials by a wider community.

In this work we present our efforts to overcome this problem. We provide evidence that grazing incidence SHI irradiation is a reliable, easy-to-use, and precise tool to fabricate various unique nanostructures in 2D materials. As a model system for our comprehensive study we used MoS_2, arguably at present the most important representative of the class of TMDCs. We demonstrate that our approach offers a versatile tool-box to efficiently fabricate nanostructures with a great degree of control by showing that the number, length, and orientation of each of these nanostructures with respect to the MoS_2 lattice may be chosen at will. In the following, we will first describe in detail the conditions for fabrication of the various nanostructures. In the second part of the paper, we focus on elucidating the physical mechanism underlying the fabrication of nano-incisions in ultra-thin MoS_2. This allows us to determine the minimum energy per path length required for an incision to occur which is an important factor with respect to the general feasibility of the technique.

2. Results

We start by presenting the basic types of modification which can be fabricated in ultra-thin MoS_2 sheets supported on SiO_2 by SHI irradiation under grazing incidence. Both of these modifications, i.e. nano-incisions and foldings, are shown in figure 1.

Here, two mechanically exfoliated samples have been irradiated using 91 MeV Xe ions under a grazing incidence angle of $\Theta = 1°$ with respect to the surface. The corresponding energy deposited per track length into the target material is usually given in terms of the electronic stopping force $S_e = dE/dx$, which amounts to 19 keV nm^{-1} in this case [17]. This energy deposition results either in the formation of incisions (which we will discuss in more detail further below), with an average length of 500 nm as shown in figure 1(b) or in the formation of foldings, figure 1(c) which appear to be similar to those found in graphene, see figure 1(e). However, in contrast to graphene, where foldings are the rule for grazing incidence irradiations [18], for foldings to be fabricated in ultra-thin MoS_2, very specific conditions have to be met. Foldings do only occur if the azimuthal angle φ between the SHI trajectory and a low-indexed direction of a MoS_2 flake is quite an exact multiple of 30°. Two examples of this phenomenon are shown in figures 2(a) and (b) in which φ is $90° \pm 3°$. If the azimuthal angle φ is just slightly off, as in figure 2(c) with $62° \pm 3°$, the resulting modifications are incisions with two notable exceptions: a small folding which might have been caused by a local irregularity, e.g. a contamination, and one large folding who's origin is explained further below. Note, that there are two uncertainties in this analysis, which result in the relatively large error bar. First, as φ is determined from AFM topography images, small drift effects due to the piezoelectric positioning system are always present and are difficult to avoid completely. Second, the edges of exfoliated MoS_2 flakes are not always straight, but can be heavily bent reducing the number of samples available for this analysis.

This unexpected dependence on the azimuthal angle is further corroborated by data obtained from bilayer MoS_2 as shown in figure 3. In basically every irradiated bilayer MoS_2 we studied, incisions were fabricated (see figure 3(a)). Only in a rare case, shown in figure 3(b), where the SHI ion hit the bilayer flake with an exact angle of $\varphi = 60°$, the formation of foldings did occur. The foldings are rather small, and exhibit a symmetry showing multiples of 30° with respect to the low-indexed MoS_2 edge. The latter finding being similar to what has been found in graphene for incidence angles Θ larger than 1° [18]. Even in case of exact alignment of the azimuthal angle φ the folding efficiency is clearly less than one: in the inset of figure 3(b) one can see an example, where an SHI impact occurred, that did not result in a folding, instead it appears as if the folding process has stopped halfway through. A lower folding efficiency has been observed for bilayer graphene as well. In the case of graphene, this can be attributed to the fact that bilayer graphene is more resistant to ion irradiation [19] and without vacancy defects usually no foldings occur in the material due to its superior mechanical strength which overcomes the upwards push from the substrate material below. However, in bilayer MoS_2, SHI do create incisions (see figure 3(a)) which should still facilitate the formation of foldings.

From the data presented above we deduce that the orientation of the SHI trajectory with respect to the MoS_2 crystallite is crucial when either foldings or incisions are to be created, and that foldings are basically limited to single layers. These findings are in striking contrast to graphene, where foldings can be fabricated even in trilayers (although with a strongly reduced efficiency) and in practically any direction with respect to the graphene lattice [15]. One obvious reason for the suppression of foldings in bilayer MoS_2—which with S–Mo–S as a building block is actually a double trilayer of atoms—is the fact, that bilayer MoS_2 is already much heavier per unit area as bilayer graphene or single layer MoS_2. The pressure exerted from the substrate during the folding process may thus simply be insufficient to push the material upwards. However, as even more important we consider the fact, that due to the additional inter-plane interactions, the de-facto trilayer MoS_2 is extremely resistant against out-of-plane bending compared to the one-atom thick graphene. Theoretical studies found a significantly larger elastic bending modulus of 9.61 eV for single layer MoS_2 compared to 1.4 eV for graphene [20], in agreement with experimental studies [21, 22]. This is in

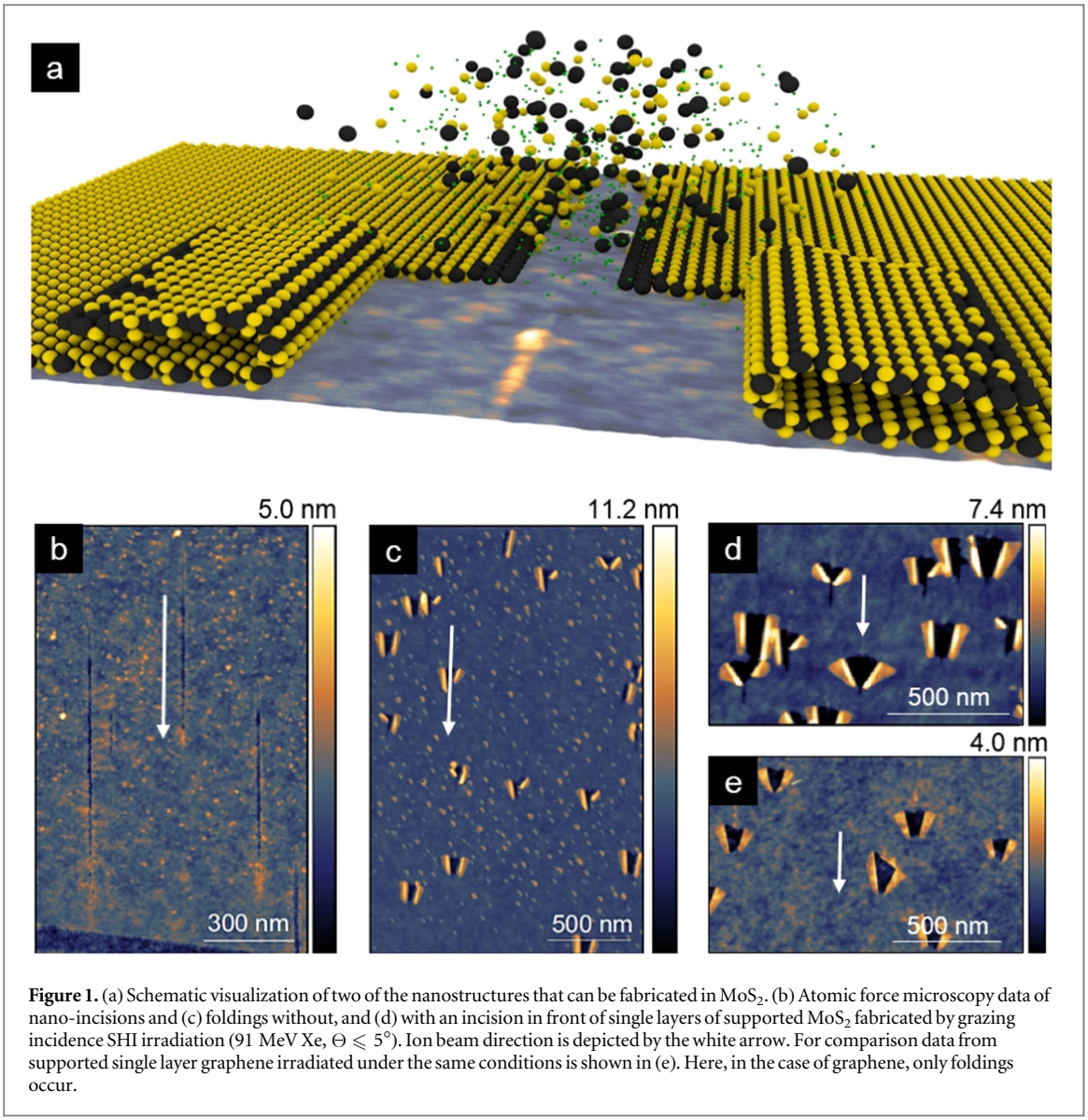

Figure 1. (a) Schematic visualization of two of the nanostructures that can be fabricated in MoS_2. (b) Atomic force microscopy data of nano-incisions and (c) foldings without, and (d) with an incision in front of single layers of supported MoS_2 fabricated by grazing incidence SHI irradiation (91 MeV Xe, $\Theta \leqslant 5°$). Ion beam direction is depicted by the white arrow. For comparison data from supported single layer graphene irradiated under the same conditions is shown in (e). Here, in the case of graphene, only foldings occur.

perfect agreement with our findings here. In addition, our data clearly point towards a directional dependence of the bending resistance: folding does become possible when the bending occurs over a low-indexed direction.

As obviously the resistance of the material against bending sets an intrinsic limit to the folding efficiency, a way to overcome this and to force foldings nevertheless, is to have two incisions running very closely together as shown in figures 2(c) and (d). By analyzing the image carefully it can be seen that this folding is indeed due to a coincidental double impact. The first SHI impact had already weakened the single layer MoS_2 flake by creating an incision (which in fact continues behind the folding, figure 2(c)) and a second SHI running very close to the first was then able to cause the folding. The chance for overlapping incisions can be drastically enhanced by crossed beam irradiations, an example of which is shown in figure 2(e). Here, a bilayer of MoS_2 has been irradiated two times with 91 MeV Xe ions under a grazing incidence angle of $\Theta = 1.5°$. Between the two irradiations, the azimuthal angle has been rotated by $\Delta\varphi = 15°$. The MoS_2 folds only and exactly at those positions, where the two incisions created by the SHI cross each other. Interestingly, in figure 2(e) two foldings are pointing backwards (events marked with 1), i.e. against the direction of the ion beam, and one is pointing forwards (event marked with 2). From a closer inspection one can learn that the position of the crossover between the two ion trajectories actually determines the direction of the folding. If the second ion crosses a incision at its beginning (event 2), the material folds in the direction of the ion trajectory and if it crosses the incision at the end (events 1), the material folds against the direction of the ion beam. Furthermore, it can be seen that the foldings pointing forwards appear flat at the folding edge, while the foldings pointing backwards exhibit pronounced folding edges. A possible reason for the flat folding edge is that the MoS_2 sheet in these forced foldings is not bent but rather broken, resulting in an

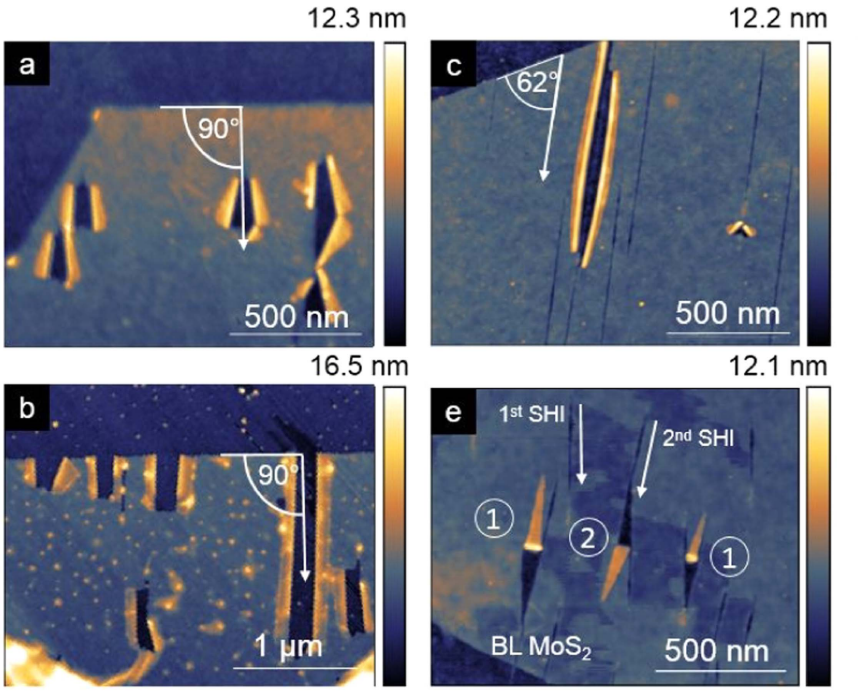

Figure 2. Single layer MoS_2 samples irradiated with 91 MeV Xe ions ($S_E = 19$ keV nm^{-1}) under grazing incidence angle $\Theta \leqslant 5°$. (a) and (b) impinging SHI trajectory with azimuthal angle $\varphi = 90° \pm 3°$ with respect to the MoS_2 edge yields foldings. (c) SHI trajectory with azimuthal angle $\varphi = 62° \pm 3°$ yields nano-incisions. The exceptional large folding is created by a double-hit as can be seen from (d), a non-contact AFM topography zoom-in on the white box marked in (c). (e) A single irradiation fabricates incisions, while two subsequent irradiations at different azimuthal angles can be used to fabricate foldings despite the materials unusually high bending resistance.

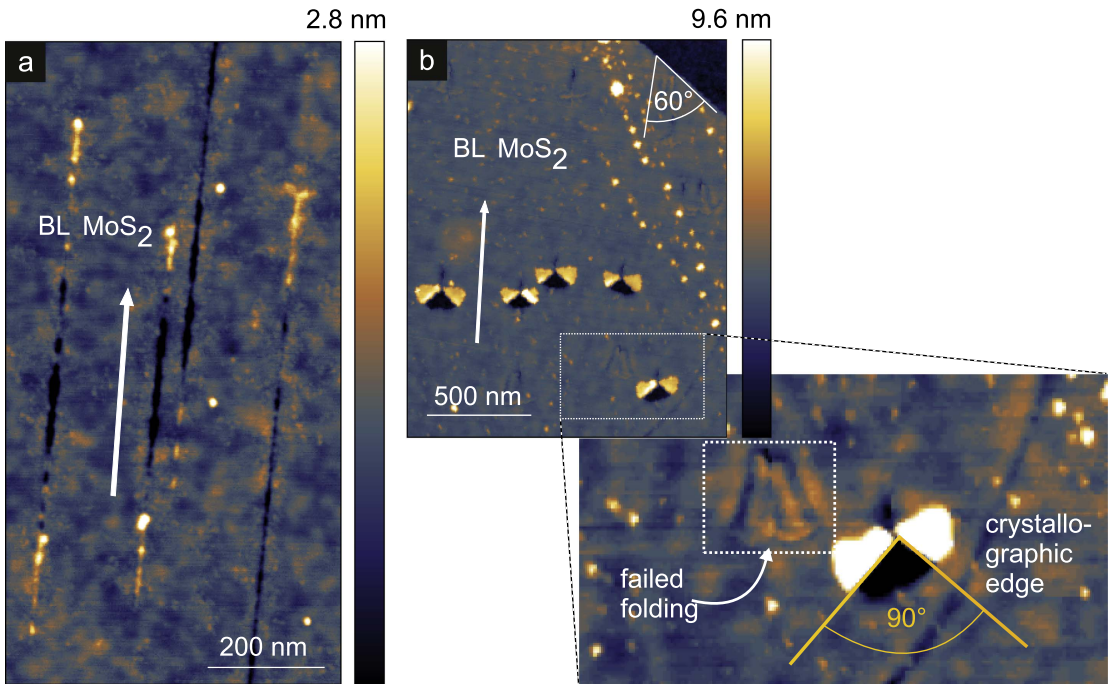

Figure 3. Swift heavy ion irradiation of bilayer MoS_2 (91 MeV Xe, $S_e = 19$ keV nm^{-1}, $\Theta \leqslant 2°$). (a) In general, SHI irradiation of MoS_2 bilayers leads to the creation of nano-incisions. (b) In one rare case, where the impinging SHI had exactly an azimuthal angle of $\varphi = 60°$, foldings were created. The inset shows a zoom-in onto a failed folding; the foldings form closed bilayer edges with multiples of 30°.

open bilayer MoS_2 edge. Similar to grown MoS_2 nano-islands [23] or other artificial MoS_2 nanostructures [24, 25], such a synthetic MoS_2 nano-flake would exhibit three chemically active edges, however not necessarily with the same crystallographic orientation.

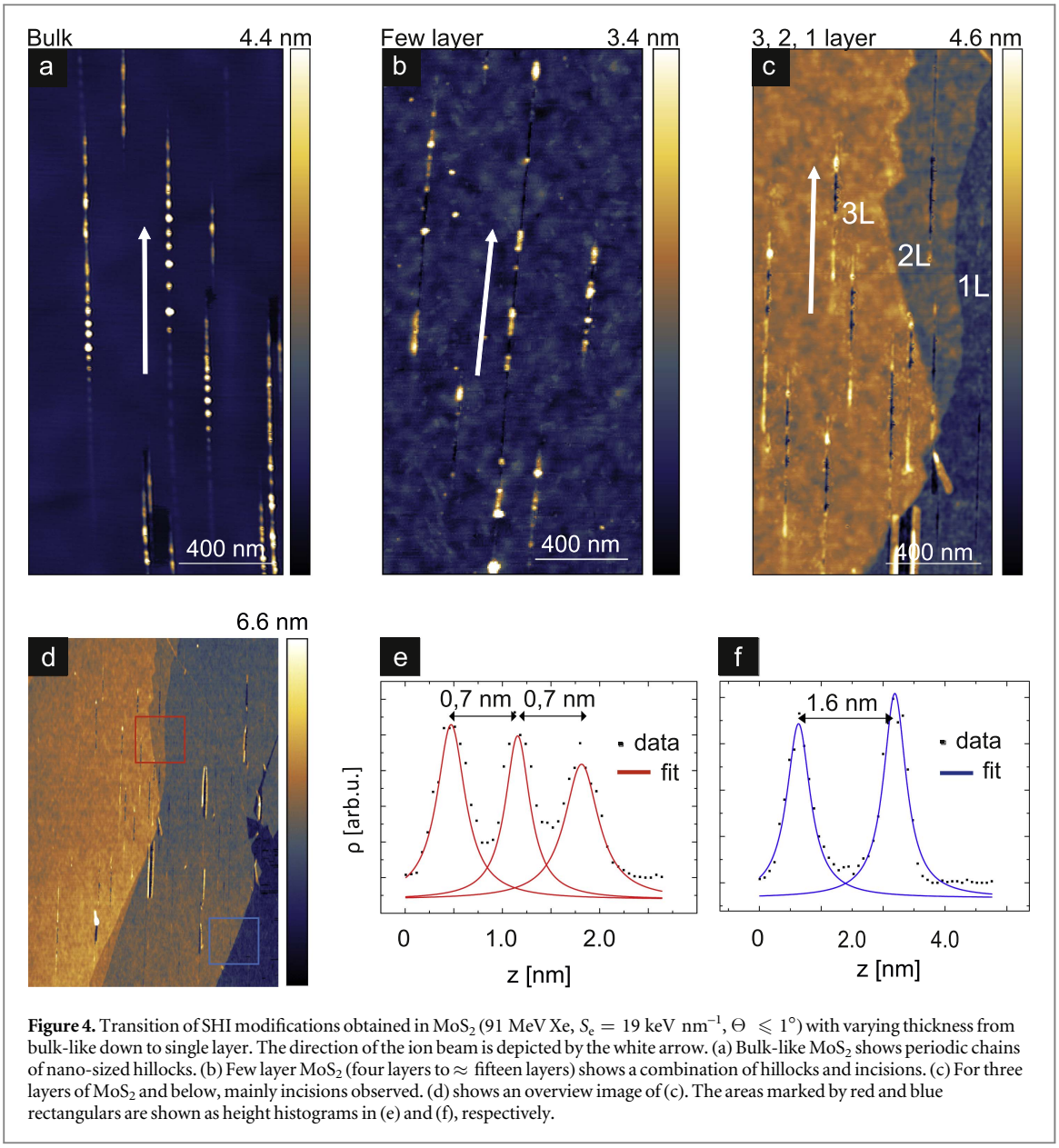

Figure 4. Transition of SHI modifications obtained in MoS_2 (91 MeV Xe, $S_e = 19$ keV nm^{-1}, $\Theta \leqslant 1°$) with varying thickness from bulk-like down to single layer. The direction of the ion beam is depicted by the white arrow. (a) Bulk-like MoS_2 shows periodic chains of nano-sized hillocks. (b) Few layer MoS_2 (four layers to $\approx$ fifteen layers) shows a combination of hillocks and incisions. (c) For three layers of MoS_2 and below, mainly incisions observed. (d) shows an overview image of (c). The areas marked by red and blue rectangulars are shown as height histograms in (e) and (f), respectively.

Next, we will focus our attention on the incisions, a novel feature which may be fabricated by SHI grazing incidence irradiation. As a consequence of the current most commonly used production processes for SL-MoS_2, i.e. mechanical exfoliation and chemical vapor deposition, respectively, very often also few layers of MoS_2 will be present at least in some parts of the sample. We have therefore investigated how the modifications due to SHI irradiation depend on the layer thickness. To this end, we have irradiated a series of MoS_2 samples with varying thickness with 91 MeV Xe ions under a grazing incidence angle of $\Theta \leqslant 1°$ and with a constant stopping force of 19 keV nm^{-1}. The AFM images in figure 4 show how the track morphology in MoS_2 evolves with decreasing layer thickness from bulk-like MoS_2 (a) down to tri-, bi- and single layer MoS_2 (c). Figure 4(d) depicts the zoom-out of figure 4(c) with the corresponding height histograms of the tri-, bi- and single layer MoS_2 in (e) and (f). Due to trapped water in between the substrate and the Mos_2, we observe an increased layer thickness of 1.6 nm for the first layer [26]. The next two layers show the typical height value of 0.7 nm [27].

In the case of bulk-like MoS_2 (measured height over 50 nm) chains of nanosized hillocks protrude from the surface. They are exactly aligned along the direction of the SHI beam and from the nominal fluence of 5 ions μm^{-2} we deduce that each chain corresponds to a single ion trajectory. In most cases, the hillocks are evenly spaced (average distance 60 ± 10 nm), their height is up to 8 nm, and their average diameter is 24 ± 3 nm. The length of this kind of surface track also varies with the angle of incidence (see below). At $\Theta \approx 0.5°$ as shown in figure 4(a), the average length of the chain of nano-hillocks is about one micron (1040 ± 275 nm). Elongated tracks have been observed in bulk MoS_2 also after irradiation with 4 MeV C_{60} ions at $\Theta \leqslant 20°$,

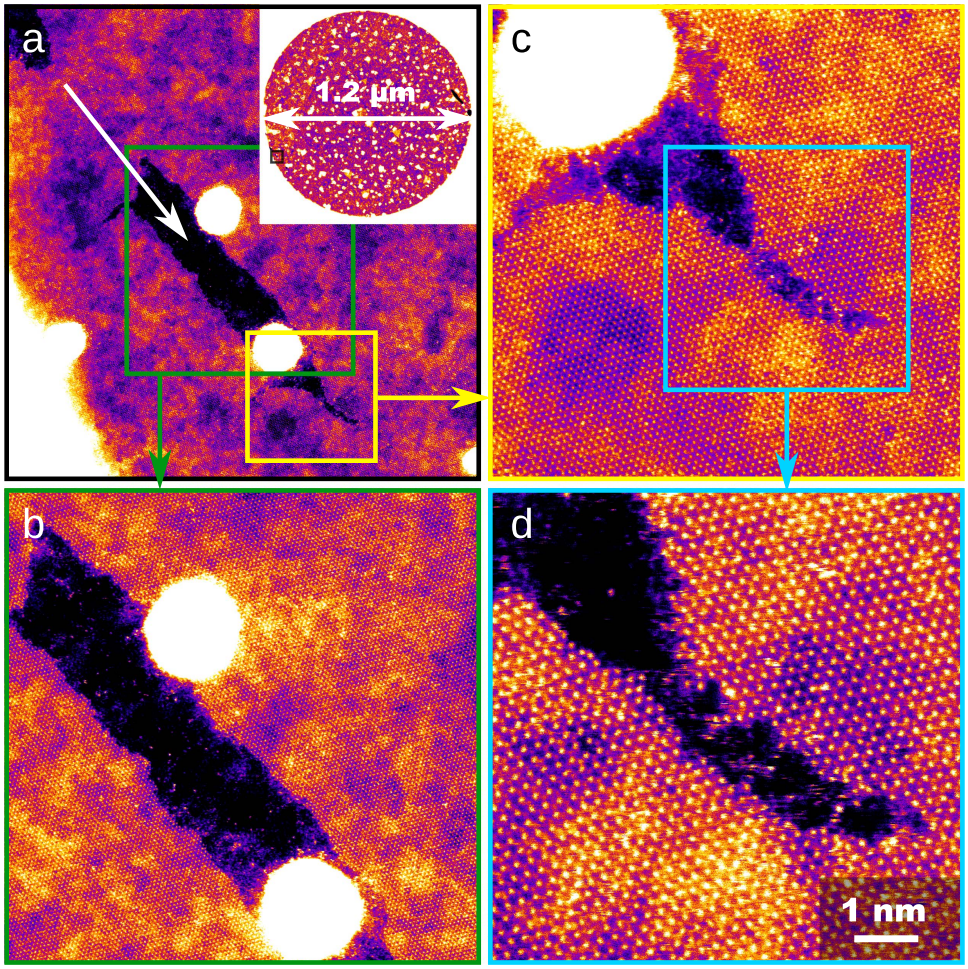

Figure 5. STEM–MAADF images taken from irradiated (91 MeV Xe, nominal angle of incidence $\Theta \leqslant 0.2°$) freestanding single layer of MoS_2 suspended on a TEM grid with holes of one micron diameter as shown in the inset in (a). The direction of the ion beam is depicted by the white arrow. The brighter features are most likely remnants of the chemicals used in the production of suspended MoS_2, see methods. The black stretch seen in (a) and (b) is a part of an incision cut into the MoS_2 sheet by the projectile. The part visible in (a) and (b) is roughly 20 nm long. The round white spots are polycrystalline and/or disordered, and have an apparent lattice spacing between 2.8 and 3.2 Å, consistent with them being Mo clusters (the spacing between lattice planes in bcc Mo varies between 2.23 and 3.85 Å, depending on the orientation). (b)–(d) Atomically resolved images of the incision show that the MoS_2 lattice outside of the ion track remains intact.

however individual hillocks were absent in these studies [28]. The striking periodicity of the hillocks found here has been observed in several crystalline materials and a possible explanation in terms of a varying electronic density in-between crystal layers has been discussed in detail in [29]. This feature disappears almost completely in thin, few layer MoS_2 sheets (thickness under 10 nm)—although individual hillocks are still created. The surface track is now a mixture of irregularly formed hillocks/protrusions and incisions, the latter of which resemble the ones found in single- and bilayer MoS_2, see figures 1(b) and 3(a).

In even thinner MoS_2 crystallites, three layers and below, the major part of the surface track consists of a continuous incision. The length of the incision varies between trilayer (3L), bilayer (2L) and single layer (1L) as shown in figure 4(c). The surface tracks in tri- and bilayer MoS_2 are accompanied by protrusions before and after the central incision. Single layer MoS_2 surface tracks generally consist of incisions only and do not show any protrusions. While the complete surface track length in these three different MoS_2 samples is comparable, the length of the incisions is reduced by ≈25% for a bilayer and by ≈50% for a trilayer. Moreover, the morphology of the incisions changes as well. While the incisions in a single layer usually appear as a clean cut with straight edges (see figure 1(b)), bilayer and trilayer incisions appear more irregular. In particular for the trilayer in figure 4(c), it can be seen that the incisions appear more like a series of roundish holes with a diameter of about 10 nm each.

The data presented above immediately leads to an interesting question from a physics as well as from an application point of view: How does the substrate influence the fabrication of incisions in SL-MoS_2? The substrate does indeed play a decisive role, as we will show further below, but it is by no means a prerequisite. In figure 5 we show scanning transmission electron microscopy (STEM) medium-angle-angular-dark-field (MAADF) images from freestanding layers

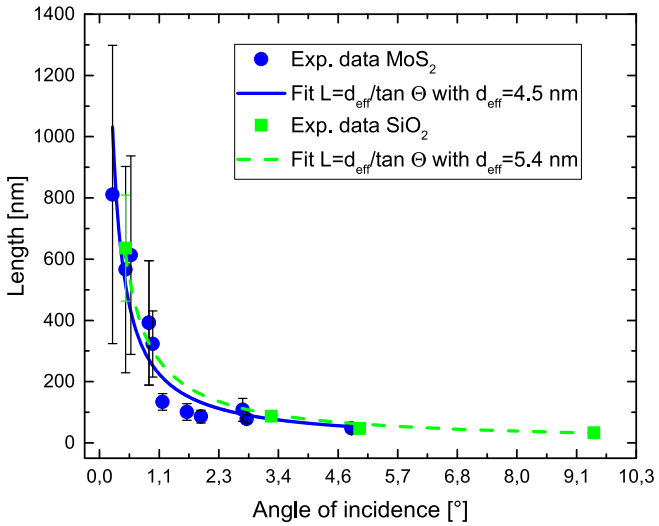

Figure 6. Plot of the incision length in irradiated single layer MoS_2 (blue dots) as a function of incidence angle Θ, 91 MeV Xe with $S_e = 19$ keV nm^{-1} and 84 MeV Ta with $S_e = 18$ keV nm^{-1}) and the surface track length in the SiO_2 substrates (green squares). Each data set has been fitted with $L = d_{\text{eff}} \tan \Theta$ (solid and dashed lines). The parameter d_{eff} denotes the depth of the projectile at which the surface track formation ends.

of MoS_2 irradiated with SHI under grazing incidence. Also here, extended incisions oriented along the direction of the incoming ion beam can be found (figure 5(a)). In comparison they are however much smaller (length typically 100 nm, i.e. about one order of magnitude) and the chance for production is much less likely (here 1 track at a fluence of 15 ions μm^{-2}). Atomically resolved images (figure 5(b)) show that the incisions are extremely narrow (less than 10 nm) and with relatively straight edges on an atomic scale. Surprisingly, the surrounding lattice remains basically undisturbed despite the violent atomic displacements that have taken place inside the ion track core.

Summarizing this part, we have demonstrated that SHI irradiation of bulk-like MoS_2 (corresponding to SL-MoS_2 deposited onto a MoS_2 substrate) will result in nano-hillocks while incisions are reliably written into single-, bi-, and trilayers of MoS_2 deposited onto SiO_2 substrates, and to a lesser degree also into free-standing MoS_2. In the transition regime of four to fifteen SiO_2-supported layers, incisions still constitute a major part of the surface track.

3. Discussion

In the following, we will discuss the possible mechanisms for the fabrication of incisions in ultrathin MoS_2, as they constitute the typical nanostructure following SHI grazing incidence irradiation. The large difference in incision sizes observed in supported and suspended MoS_2, respectively, obviously points towards the substrate as a major driving force. The same can be deduced from the analysis of the incision length with respect to the angle of incidence. The corresponding experimental data is presented in figure 6 (blue dots). We assume that the traversing ion initiates the primary electronic excitations and that the subsequent processes will affect the material around the trajectory. Whatever changes are induced, they will be most pronounced in the immediate vicinity of the trajectory while further away the changes are less severe. At some given distance, basically the radius of the affected volume (on the order of a few nanometers), changes will no longer be effective and observable, respectively. If, like in our case, the ion traverses the surface under an angle, this radius will correspond to an effective depth d_{eff} where the primary process can take place and its consequences may still be detected at the surface by an AFM for instance. We can then fit the data from figure 6 by the geometrical relation $L = d_{\text{eff}}/\tan\Theta$. The best fit (blue line in figure 6) is obtained for $d_{\text{eff}} = 4.5$ nm, which is a typical value for dielectrics [29, 30].

The key point here however is, that d_{eff} is significantly larger than the thickness of a single layer MoS_2 which is ≈1 nm. It is therefore evident that the processes yielding the incisions in supported SL-MoS_2 cannot take place exclusively in the MoS_2 but must occur mainly in the substrate material. We therefore need to consider what happens in the SiO_2 when the ion passes through, and how this affects the SL-MoS_2. As already mentioned, the direct collision of a SHI with the target atoms is negligible in this energy range. Instead, during its passage through matter an SHI excites the electrons of the target material by direct ionization and secondary electron creation which then propagate through the target. Several mechanisms for material modifications related to the electronic excitation due to electronic stopping have been proposed. In particular, these are Coulomb explosion as a consequence of the electrostatic repulsive forces between the atoms in the ionized region [31–33], exciton self-

trapping causing a local lattice distortion [34], non-thermal melting caused by significant changes of the interatomic potentials [35], or phase transitions such as melting due to a thermal spike [36, 37]. These mechanisms occur on vastly different time scales, ranging from a few fs in the case of processes related to non-thermalized electrons up to ps in the case of phase transitions.

In non-metallic systems the resulting modifications are very often permanent in nature and are thus easily detectable (for a review see e.g. [38]), in the case of graphene see e.g. [39]. After irradiation under grazing incidence, hillock chains, or more general, protruding surface tracks, are frequently observed in crystalline dielectrics or graphite [13, 29, 40–43]. The surface tracks which are shown in figure 4(a) in bulk MoS_2 bear a striking resemblance to the ones found in e.g. $SrTiO_3$. For $SrTiO_3$ in particular, the origin of these hillock chains has been successfully explained in terms of a thermal spike model, i.e. the hillocks consist of re-solidified molten material. For MoS_2 a rather low decomposition temperature of $T_c \approx 1460$ K has been reported [44, 45]. This and the similarity in morphology leads us to believe that also the hillock chains in bulk-like MoS_2 consist of (potentially non-stoichiometric) MoS_2 which has re-solidified after a phase transition caused by the thermal spike. In thin layers of MoS_2 instead of hillocks, incisions are formed and therefore a different mechanism must be in effect. On the basis of the previous observation that the process cannot take place in the ultra-thin MoS_2 alone, we put forward the following hypothesis for the incision formation in supported MoS_2: a thermal spike in the SiO_2 substrate results in a super heated surface track and in areas, where the temperature of the surface track in SiO_2 reaches or even exceeds the decomposition temperature of MoS_2, and thus material is evaporating from the track region leaving nanoscaled incisions behind. To test our hypothesis, the corresponding track length in SiO_2 samples have been measured as well. The data (green squares in figure 6) are in good agreement with our hypothesis. Furthermore, the difference in the effective depth determined from the two fits corresponds roughly with the thickness of the MoS_2 layer, which further corroborates our hypothesis.

Note that preferred sublimation of one atom species may occur. Previous studies of thermally induced desorption found that S_2 vaporization starts already at 1140 K and in the presence of water decomposition may occur at even lower temperatures (565 K) due to the vaporization of SO_2. The lattice temperature in the spike is definitely high enough to decompose MoS_2 but in the border region, where temperatures are lower, preferentially sulfur atoms may evaporate which would be beneficial for any potential catalytic activity [46, 47] of the incision but also with respect to the interesting optical and electronic properties of metallic edge states in MoS_2 [48, 49]. In order to estimate the minimum energy required to fabricate an incision, one can simply look into the available data for track formation in SiO_2, as e.g. found in [50]. From this we infer that a stopping force of 2 keV nm^{-1} would be already sufficient. Note that this is the threshold for grazing incidence and it can thus not be directly compared to previous work on SHI and proton irradiation of MoS_2 field effect transistors, where it was shown that the devices withstand surprisingly high fluences at much higher stopping forces before deterioration [51, 52]. Finally, we wish to point out that up-scaling to large area samples or down-scaling to localized single ion hits [53] is entirely possible with our approach which opens up ample possibilities for applications. In particular, it remains to be seen whether SHI causes direct damage in freestanding SL-MoS_2 also under non-glancing angles which would due to the resulting minute pore size immediately pave the way to exciting experiments such as the fabrication and study of synthetic nanopores for DNA sequencing. Furthermore, we expect that other 2D-TDMCs, in particular $MoSe_2$, WS_2 and WSe_2, will show a very similar response towards SHI irradiation.

In conclusion, we have shown that by choosing the proper irradiation conditions, two distinct morphological changes can be fabricated in single layers of MoS_2 by individual ions, namely foldings and incisions. Folding is significantly suppressed in MoS_2 due to its high bending resistance, but can still be routinely obtained by either exploiting the directional dependence of the bending resistance or by crossed-beam irradiations. The incisions represent a novel feature and are unique to the crystalline 2D semiconductor as surface tracks in the 3D form manifest themselves as material protruding from the surface which is the typical morphology for surface tracks in bulk dielectrics. The widths of the incisions in supported samples is around 10 nm while their aspect ratio (width:length) can be tuned from more than 1:1000 down to nanopores with a ratio of 1:1. Incisions in suspended single layers are found to be one order of magnitude smaller in length. For supported MoS_2 the formation mechanism of the incisions could be linked to an ion induced thermal spike in the SiO_2 substrate.

4. Methods

Sample preparation

Supported samples have been prepared via mechanical exfoliation from a bulk single crystal of MoS_2 (Molykote). Suspended samples were produced by transferring CVD-grown MoS_2 onto a TEM grid. At first, single crystal MoS_2 flakes were grown directly on a 300 nm SiO_2/Si substrate by CVD. A 1% sodium cholate solution is initially spin coated onto the SiO_2 substrate to act as a growth promoter. A micro droplet of a saturated solution of Ammonium heptamolybate (AHM) is deposited onto the corner of the substrate.

The AHM will act as the Molybdenum feedstock. The substrate is placed in the center of a 1 inch Lindberg blue furnace and 15 mg of sulfur is placed upstream at a distance of 18 cm from the growth substrate. 500 sccm of Nitrogen is flown through the chamber and the temperature of the furnace is ramped up to 800 °C, the sulfur pellet is heated up to 150 °C. After a 30 min growth, the furnace is then stopped and rapidly cooled. The growth substrate is retrieved and MoS_2 flakes were grown across the SiO_2 substrate. Then, a thin Poly(methyl methacrylate) layer (PMMA, ARP 671.05; ALLRESIST GmbH) is spin coated on the MoS_2 sample (30 sec, 1000 rpm) and annealed under ambient conditions (150 °C, 4 min). The wafer is then placed onto the surface of a KOH solution (3 g of KOH and 50 ml DI water) which etches the SiO_2 away so that the PMMA/MoS_2 detaches from the wafer. After replacing the etchant with DI water one can gradually reduce the amount of the liquid letting the PMMA/MoS_2 stack sink onto the TEM grid. The remaining PMMA is dissolved in a bath of acetone for 45 min.

Irradiation

The irradiation with SHI took place at the large scale facilities GANIL in Caen, France. MoS_2 on SiO_2 has been irradiated with 91 MeV Xe ($S_e = 19$ keV nm^{-1}) and 84 MeV Ta ($S_e = 18$ keV nm^{-1}) with typically 10 ions μm^{-2} at varying angles of incidence in the range from 0.25° to 5° with an accuracy of 0.2° (see [14] for details). Suspended MoS_2 samples have been irradiated with 93 MeV Xe ions at a nominal fluence of 15 ions μm^{-2} and at an angle of incidence of $0.2 \pm 5°$. Due to the nature of these samples a more accurate control of the angle of incidence is currently not possible, which also prevents a more systematic analysis of the freestanding samples at this point.

Imaging

Atomic force microscopy images were taken at the University of Duisburg-Essen with a Veeco Dimension 3100 AFM using Nanosensors NCHR tips for the measurements in ambient conditions. The STEM experiments were carried out with an aberration corrected Nion UltraSTEM 100 microscope in Vienna. The microscope was operated at 60 kV in near ultra-high vacuum ($\sim 2 \times 10^{-7}$ Pa). The beam convergence semiangle was 30 mrad and the semi-angular range of the MAADF detector was 60–200 mrad.

Acknowledgments

OO, LM and MS thank the DFG for financial support within the SPP 1459 'Graphene'. We thank M Karlusic for fruitful and ongoing discussions and S Akcöltekin for analysis of the SiO_2 samples. JK acknowledges funding from the Wiener Wissenschafts-, Forschungs- und Technologiefonds (WWTF) via project MA14-009. CHN and ATCJ acknowledge support from the US National Science Foundation, through the EFRI 2DARE program, Grant #EFMA-1542879.

References

[1] Lv R, Robinson J A, Schaak R E, Du S, Sun Y, Mallouk T E and Terrones M 2015 Transition metal dichalcogenides and beyond: synthesis, properties, and applications of single- and few-layer nanosheets *Accounts Chem. Res.* **48** 56–64

[2] Wang F, Wang Z, Wang Q, Wang F, Yin L, Xu K, Huang Y and He J 2015 Synthesis, properties and applications of 2D non-graphene materials *Nanotechnology* **26** 292001

[3] Feng J, Liu K, Bulushev R D, Khlybov S, Dumcenco D, Kis A and Radenovic A 2015 Identification of single nucleotides in MoS_2 nanopores *Nat. Nanotechnol.* **10** 1070–6

[4] Heiranian M, Farimani A B and Aluru N R 2015 Water desalination with a single-layer MoS_2 nanopore *Nat. Commun.* **6** 8616

[5] Yang Y, Fei H, Ruan G, Xiang C and Tour J M 2014 Edge-oriented MoS_2 nanoporous films as flexible electrodes for hydrogen evolution reactions and supercapacitor devices *Adv. Mater.* **26** 8163–8

[6] Koperski M, Nogajewski K, Arora A, Cherkez V, Mallet P, Veuillen J-Y, Marcus J, Kossacki P and Potemski M 2015 Single photon emitters in exfoliated WSe_2 structures *Nat. Nanotechnol.* **10** 503–6

[7] Ding Z, Pei Q-X, Jiang J-W and Zhang Y-W 2015 Manipulating the thermal conductivity of monolayer MoS_2 via lattice defect and strain engineering *J. Phys. Chem.* C **119** 16358

[8] Mignuzzi S, Pollard A J, Bonini N, Brennan B, Gilmore I S, Pimenta M A, Richards D and Roy D 2015 Effect of disorder on Raman scattering of single-layer MoS_2 *Phys. Rev.* B **91** 195411

[9] Komsa H-P, Kotakoski J, Kurasch S, Lehtinen O, Kaiser U and Krasheninnikov A V 2012 Two-dimensional transition metal dichalcogenides under electron irradiation: defect production and doping *Phys. Rev. Lett.* **109** 035503

[10] Kang N, Paudel H P, Leuenberger M N, Tetard L and Khondaker S I 2014 Photoluminescence quenching in single-layer MoS_2 via oxygen plasma treatment *J. Phys. Chem.* C **118** 21258–63

[11] Avasthi D K and Mehta G K 2011 *Swift Heavy Ions for Materials Engineering and Nanostructuring,* (*Springer Series in Materials Science* vol 145) (Netherlands: Springer)

[12] Sigmund P 2008 *Particle Penetration and Radiation Effects: General Aspects and Stopping of Swift Point Charges* (*Springer Series in Solid-State Sciences* vol 151) (Berlin: Springer)

[13] Akcöltekin E, Peters T, Meyer R, Duvenbeck A, Klusmann M, Monnet I, Lebius H and Schleberger M 2007 Creation of multiple nanodots by single ions *Nat. Nanotechnol.* **2** 290–4

[14] Ochedowski O, Osmani O, Schade M, Bussmann B K, Ban-d'Etat B, Lebius H and Schleberger M 2014 Graphitic nanostripes in silicon carbide surfaces created by swift heavy ion irradiation *Nat. Commun.* **5** 3913

[15] Akcöltekin S, Bukowska H, Peters T, Osmani O, Monnet I, Alzaher I, Ban d'Etat B, Lebius H and Schleberger M 2011 Unzipping and folding of graphene by swift heavy ions *Appl. Phys. Lett.* **98** 103103

[16] Ochedowski O, Bukowska H, Freire Soler V M, Bröckers L, Ban-d'Etat B, Lebius H and Schleberger M 2014 Folding two dimensional crystals by swift heavy ion irradiation *Nucl. Instr. Meth. B* **340** 39–43

[17] Ziegler J F, Ziegler M D and Biersack J P 2010 SRIM—the stopping and range of ions in matter *Nucl. Instr. Meth.* B **268** 1818–23

[18] Ochedowski O, Lehtinen O, Kaiser U, Turchanin A, Ban-d'Etat B, Lebius H and Schleberger M 2015 Nanostructuring graphene by dense electronic excitation *Nanotechnology* **26** 465302

[19] Kumar S, Tripathi A, Singh F, Khan S A, Baranwal V and Avasthi D K 2014 Purification/annealing of graphene with 100 MeV Ag ion irradiation *Nanoscale Res. Lett.* **9** 126

[20] Jiang J W 2014 The buckling of single-layer MoS_2 under uniaxial compression *Nanotechnology* **25** 355402
[21] Bertolazzi S, Brivio J and Kis A 2011 Stretching and breaking of ultrathin MoS_2 *ACS Nano* **5** 9703–9
[22] Castellanos-Gomez A, Poot M, Steele G A, van der Zant H S J, Agrait N and Rubio-Bollinger G 2012 Elastic properties of freely suspended MoS_2 nanosheets *Adv. Mater.* **24** 772–5
[23] Bruix A, Fuchtbauer H G, Tuxen A K, Walton A S, Andersen M, Porsgaard S, Besenbacher F, Hammer B and Lauritsen J V 2015 *In situ* detection of active edge sites in single-layer MoS_2 catalysts *ACS Nano* **9** 9322–30
[24] Kibsgaard J, Chen Z, Reinecke B N and Jaramillo T F 2012 Engineering the surface structure of MoS_2 to preferentially expose active edge sites for electrocatalysis *Nat. Mater.* **11** 963–9
[25] Yang L, Hong H, Fu Q, Huang Y, Zhang J, Cui X, Fan Z, Liu K and Xiang B 2015 Single-crystal atomic-layered molybdenum disulfide nanobelts with high surface activity *ACS Nano* **9** 6478–83
[26] Schumacher A, Scandella L, Kruse N and Prins R 1993 Single-layer MoS_2 on mica: studies by means of scanning force microscopy *Surf. Sci. Lett.* **289** L595–598
[27] Radisavljevic B, Radenovic A, Brivio J, Giacometti V and Kis A 2011 Single-layer MoS_2 transistors *Nat. Nanotechnol.* **6** 147–50
[28] Henry J, Dunlop A and Della-Negra S 1998 Craters, bumps and onion structures in MoS_2 irradiated with MeV C_{60} ions *Nucl. Instr. Meth.* B **146** 405–11
[29] Akcöltekin E, Akcöltekin S, Osmani O, Duvenbeck A, Lebius H and Schleberger M 2008 Swift heavy ion irradiation of $SrTiO_3$ under grazing incidence *New J. Phys.* **10** 053007
[30] Akcöltekin S, Akcöltekin E, Roll T, Lebius H and Schleberger M 2009 Patterning of insulating surfaces by electronic excitation *Nucl. Instr. Meth.* B **267** 1386–9
[31] Fleischer R L, Price P B and Walker R M 1965 Ion explosion spike mechanism for formation of charged-particle tracks in solids *J. Appl. Phys.* **36** 3645
[32] Bringa E M and Johnson R E 2002 Coulomb explosion and thermal spikes *Phys. Rev. Lett.* **88** 165501
[33] Cherednikov Y, Sun S N and Urbassek H M 2013 Hybrid particle-in-cell/molecular dynamics simulation of swift-ion tracks in LiF *Phys. Rev.* B **87** 245424
[34] Itoh N and Marshall Stoneham A 1998 Excitonic model of track registration of energetic heavy ions in insulators *Nucl. Instr. Meth.* B **146** 362–6
[35] Rethfeld B, Kaiser A, Vicanek M and Simon G 2002 Ultrafast dynamics of nonequilibrium electrons in metals under femtosecond laser irradiation *Phys. Rev.* B **65** 214303
[36] Toulemonde M, Dufour C and Paumier E 1992 Transient thermal process after a high-energy heavy-ion irradiation of amorphous metals and semiconductors *Phys. Rev.* B **46** 14362–9
[37] Szenes G 1995 General features of latent track formation in magnetic insulators irradiated with swift heavy ions *Phys. Rev.* B **51** 8026–9
[38] Aumayr F, Facsko S, El-Said A S, Trautmann C and Schleberger M 2011 Single ion induced surface nanostructures: a comparison between slow highly charged and swift heavy ions *J. Phys.: Condens. Matter* **23** 393001
[39] Zeng J *et al* 2016 Comparative study of irradiation effects in graphite and graphene induced by swift heavy ions and highly charged ions *Carbon* **100** 16–26
[40] Liu J, Neumann R, Trautmann C and Mueller C 2001 Tracks of swift heavy ions in graphite studied by scanning tunneling microscopy *Phys. Rev.* B **64** 184115
[41] Karlušić M *et al* 2015 Response of GaN to energetic ion irradiation: conditions for ion track formation *J. Phys. D: Appl. Phys.* **48** 325304
[42] Papaleo R M, Thomaz R, Gutierres L I, de Menezes V M, Severin D, Trautmann C, Tramontina D, Bringa E M and Grande P L 2015 Confinement effects of ion tracks in ultrathin polymer films *Phys. Rev. Lett.* **114** 118302
[43] Gruber E *et al* 2016 Swift heavy ion irradiation of CaF_2—from grooves to hillocks in a single ion track *J. Phys.: Condens. Matter* **28** 405001
[44] Yang R, Li Z, Wang Y, Yang G and Li H 2013 Synthesis and characterization of MoS_2Ti composite coatings on Ti_6Al_4V prepared by laser cladding *AIP Adv.* **3** 022106
[45] Gordon J M, Katz E A, Feuermann D, Albu-Yaron A, Levy M and Tenne R 2008 Singular MoS_2, SiO_2 and Si nanostructures— synthesis by solar ablation *J. Mater. Chem.* **18** 458–62
[46] Jaramillo T F, Jorgensen K P, Bonde J, Nielsen J H, Horch S and Chorkendorff I 2007 Identification of active edge sites for electrochemical H_2 evolution from MoS_2 nanocatalysts *Science* **317** 100–2
[47] Le D, Rawal T B and Rahman T S 2014 Single-layer MoS_2 with sulfur vacancies: structure and catalytic application *J. Phys. Chem. C* **118** 5346–51
[48] Pan H and Zhang Y-W 2012 Edge-dependent structural, electronic and magnetic properties of MoS_2 nanoribbons *J. Mater. Chem.* **22** 7280
[49] Wu D *et al* 2016 Uncovering edge states and electrical inhomogeneity in MoS_2 field-effect transistors *Proc. Natl Acad. Sci.* **113** 8583–8
[50] Benyagoub A and Toulemonde M 2015 Ion tracks in amorphous silica *J. Mater. Res.* **30** 1529–43
[51] Ochedowski O, Marinov K, Wilbs G, Keller G, Scheuschner N, Severin D, Bender M, Maultzsch J, Tegude F J and Schleberger M 2013 Radiation hardness of graphene and MoS_2 field effect devices against swift heavy ion irradiation *J. Appl. Phys.* **113** 214306
[52] Kim T-Y, Cho K, Park W, Park J, Song Y, Hong S, Hong W-K and Lee T 2014 Irradiation effects of high-energy proton beams on MoS_2 field effect transistors *ACS Nano* **8** 2774–81
[53] Jakšić M *et al* 2007 New capabilities of the Zagreb ion microbeam system *Nucl. Instr. Meth.* B **260** 114–8